Effect of Laser Remelting on Tribological Performance of Ni-Cr-B-Si Coatings Deposited by Laser Metal Deposition

Jurandir Marcos Sá de Sousa[1] , Rafael Gomes Nunes Silva[1] , Adriano de Souza Pinto Pereira[1] , Calil Amaral[1] , Milton Pereira[1]

[1] Universidade Federal de Santa Catarina – UFSC, Departamento de Engenharia Mecânica, Laboratório de Mecânica de Precisão – Laser, Florianópolis, SC, Brasil.

Abstract: Ni-superalloys coatings deposited via laser metal deposition (LMD) have been known to perform well in increasing components lifespan and consequently reducing production and repair costs. Although most of these coatings already present good results in its hardness, and tribological behavior, some can be improved by post-deposition treatments, such as laser remelting. In this ambit, the present paper aims to evaluate the laser remelting posttreatment effects on the Ni-Cr-B-Si coating sliding tribological behavior. For this, two conditions were compared: Ni-Cr-B-Si coating as-deposited and Ni-Cr-B-Si coating as-deposited and remelted. The coating's occurrence of superficial macro defects, their microhardness, and tribological performance in the pin-on-disk (ASTM G99) test were compared. Friction coefficient (load cell), volumetric loss (optical interferometry), Archard's wear coefficient and worn surfaces (SEM and EDS), were evaluated. Results show that the laser remelting posttreatment was effective in reducing cooling cracks, increasing hardness and reducing friction coefficient oscillation and volumetric loss average.

Key-words: Ni-superalloys; Laser metal deposition; Laser remelting; Tribological performance; Cooling cracks.

1. Introduction

Intense industrial growth requires constant material development to enhance the most diverse applications. Work components or implements subjected to adhesive wear are common and are no exception to the previous statement. Generally, to reduce wear, these applications need exposed surfaces with high hardness values and good roughness quality, which, by their turn, avoid the occurrence of high friction coefficients (COF), wear rates and the joint interaction between wear mechanisms (Zum Gahr, 1987; Hutchings and Shipway, 2017). This interaction accelerates the component's deterioration process, reducing their lifespan and consequently increasing repair and replacement costs. Extensive studies with estimated data relating to losses with energy consumption and components deterioration due to the deleterious action of friction and different wear mechanisms in many industrial sectors are presented in various papers of Holmberg and his collaborators: energy consumption, costs, and emissions in worldwide scale (Holmberg and Erdemir, 2017); in the mining industry (Holmberg et al., 2017); concerning the friction in passenger cars (Holmberg et al., 2012); to the friction in trucks and buses (Holmberg et al. 2014).

Coatings application with desired and specific properties have proven to be a good alternative, both operationally and financially. Such allows preparation of only the surface that will be directly exposed to wear condition, dispensing the integral component manufacture from a noble alloy, resource that drastically reduces production costs. Wear resistant coatings can be deposited by thermal spray and arc welding techniques. However, such coatings may generate, in several conditions, lack of metallurgical adhesion, extensive heat-affected zone (HAZ) and high dilution. These aspects are emphasized from well-established literature until more recent works (Toyserkani et al., 2005; Zhong and Liu, 2010; Davim, 2013; Houdková et al., 2014; Silva and D'Oliveira, 2015, 2016; Zhao et al., 2018; Sousa et al., 2020).

Literature indicates that the laser metal deposition (LMD) technique can generate coatings which are successful in facing these processing problems. LMD's advantages derive from the special laser radiation properties, which generates a highly directional beam, high maximal available power, versatility and high achievable energy density (Toyserkani et al., 2005). Ni-Cr-B-Si alloys, in their turn, it's an alloy class that's capable of simultaneously providing resistance to abrasive, adhesive and corrosive wear mechanisms (Silva and D'Oliveira, 2015, 2016; Sousa et al., 2020).

Laser remelting process is a technique belonging to the laser post-processing method (that includes, among others, remelting, texturization and heat treatments). In such a laser beam is irradiated in the target surface to remelt a thin material layer, generating a molten pool (Houdková et al., 2014; Marimuthu et al., 2015). The surface tension from this molten pool causes portions of the material`s roughness peaks to flow into valleys, making the surface more uniform, homogeneous and flat. Besides improving metallurgical aspects, which standardizes the surface thermal cycle, generating better mechanical properties

distribution along with the coating (Temmler et al., 2015). In this process, there is no removal, but only material reallocation (Yin et al., 2011; Zhao et al., 2018).

Despite the advantages highlighted, NI-Cr-B-Si alloy coatings are highly susceptible to cooling cracks appearance (Houdková et al., 2014; Silva and D'Oliveira, 2016; Sousa et al., 2020). LMD deposition process and the laser remelting posttreatment surface have high parametrization complexity due to a large number of variables involved (Davim, 2013; Houdková et al., 2014; Marimuthu et al., 2015; Pôrto et al., 2019). Thus, the present paper aims to contribute to this discussion. Utilizing a commercial Ni-Cr-B-Si alloy and a fiber laser processing system, two different conditions were prepared: Ni-Cr-B-Si coating as-deposited and Ni-Cr-B-Si coating as-deposited and remelted. Laser deposition parameters were determined based on preliminary tests performed by Sousa (2019) and Sousa et al. (2020). After sample's preparation, surface's aspects assessments, hardness and tribological behavior inference were carried out. The main objective of this paper is to understand the laser remelting posttreatment effects on the Ni-Cr-B-Si coating sliding tribological performance.

2. Experimental Procedure

Experimental procedures are divided into three steps: (1) coating deposition process; (2) application of laser remelting posttreatment in half the samples available; (3) microhardness test and pin-on-disk tribological test in dry-medium on all samples, following the ASTM-G99 (American Society for Testing and Materials, 2017b) standard requirements.

2.1. Coatings deposition process

ASTM A36 material - carbon steel drawn discs (Ø 50.0 mm × δ 10.0 mm) were used as substrate. Their surfaces were prepared by abrasive blasting process, ethyl alcohol cleaning, and drying. Coating material consists of the Ni-Cr-B-Si 1545-00 alloy manufactured by Höganäs S.A. The powder particle size range is 106±53 µm and the chemical composition is shown in Table 1.

Table 1. Ni-Cr-B-Si 1545-00 alloy chemical composition.

Chemical composition - Elements (wt.%)					
C	Fe	Cr	B	Si	Ni
0.3-0.4	2.0-3.4	7.5-10.0	1.7-2.0	3.3-3.9	Bal.

The deposition parameters choice was based on the research group (LMP-Laser) know-how with the respective laser deposition system (characteristics described in topic 2.2.) for the alloy employed as addition material (Ni-Cr-B-Si). Regarding the scanning speed, 30.0 mm/s corresponds to the maximum deposition system limit. As for the combination of power and scanning speed values, it was based on previous work carried out by the group (Sousa, 2019; Sousa et al., 2020), which, in turn, are based on the literature and on preliminary tests, whose characteristics of the observed deposits are good quality, concerning geometry and defects absence. The main consulted authors are listed below: Borges et al. (2010), Hemmati et al. (2011, 2012, 2013, 2014), Ghabchi et al. (2013), Chen et al. (2015), Kaiming et al. (2016), Stanciu et al. (2016), Weng et al. (2016) and Deschuyteneer et al. (2017). Aspects of their respective works will be discussed together with the results presented throughout this paper (topic 3.).

The coatings were deposited using a YLS-10000 IPG PHOTONICS® fiber laser source and the parameters shown in Table 2. The final coatings overlap rate, set as 30%, was chosen through simulations performed in MATLAB® software, in a program developed within the LMP-Laser group. The algorithm was developed based on the work presented by Ocelík et al. (2014).

Table 2. Deposition and remelting LMD parameters.

LMD deposition parameters						
Laser power (P)	Scanning speed (V)	Powder feed rate	Laser beam diameter	Shielding gas (Ar)	Carrier gas (Ar)	Overlap rate
1.05 kW	5.0 mm/s	10.4 g/min	0.8 mm	15.0 l/min	5.0 l/min	30%
LMD remelting parameters						
Laser power (P)	Scanning speed (V)	Powder feed rate	Laser beam diameter	Shielding gas (Ar)	Carrier gas (Ar)	Overlap rate
1.05 kW	5.0 mm/s	-	0.8 mm	15.0 l/min	5.0 l/min	30%

As work describes, all tests were performed at least twice, including the pin-on-disk tribological test. However, the sample's number was reduced due to the parameter's robustness (previously determined by Sousa, 2019). Besides that, most of the Ni-Cr-B-Si alloy (available in the laboratory) was previously consumed in the preliminary and effective tests carried out by Sousa

(2019). Given the high cost and dwell time for the respective alloy acquisition, decision to reduce the sample space was taken. Thus, it is believed that the parameter used in this paper for the as-deposited condition is adequate, due to the low dilution and defects absence (with the exception of the cooling cracks, which will be better discussed in topic 3.).

2.2. Application of laser remelting posttreatment in half the sample space

Four samples were coated with the chosen parameters: as-deposited (two samples); as-deposited and remelted (two samples). For the remelted samples preparation, the following process was executed: immediately after the coating layer deposition, the powder feed was turned off and, using only laser beam and keeping the other deposition parameters constant, the coating surface was completely swept by the laser beam (following the same trajectory as the previous deposition process, however, with the powder feed turned off), establishing the remelted layer. Figure 1 illustrates these two steps. To facilitate understanding, the coatings were divided into two categories: as-deposited and remelted.
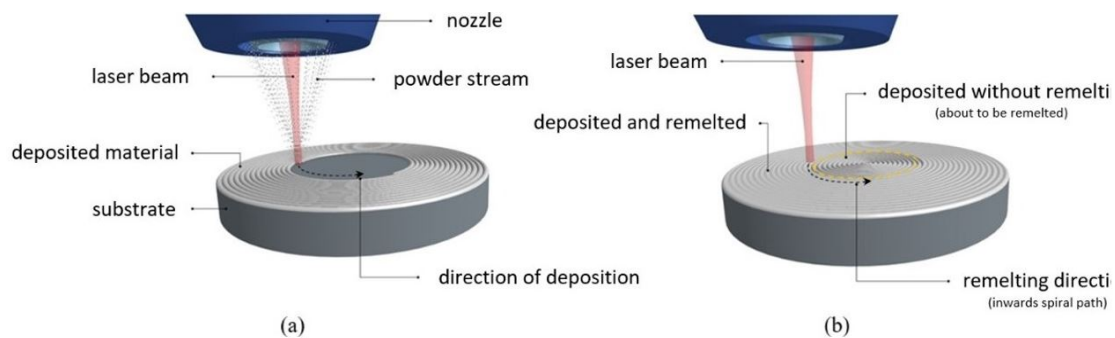
Figure 1. Deposition and remelting of the coating. (a) as-deposited and (b) remelted.

2.3. Microhardness test and pin-on-disk tribological test in dry medium

Vickers microhardness test was performed in a sample, randomly chosen, from each condition using the SHIMADZU® HMV-2TADW equipment, according to the ASTM-E92 (American Society for Testing and Materials, 2017a) standard guidelines: HV_1 scale - 10 N load for 10 s. Indentations were applied in the coating's surface in corresponding regions to the later tribological test area (radial direction), as shown in Figure 2. Spacing between indentations was 5.0 mm and 7.0 mm for the diameter 1 ($\emptyset$ 30.0 mm) and diameter 2 ($\emptyset$ 36.0 mm), respectively.
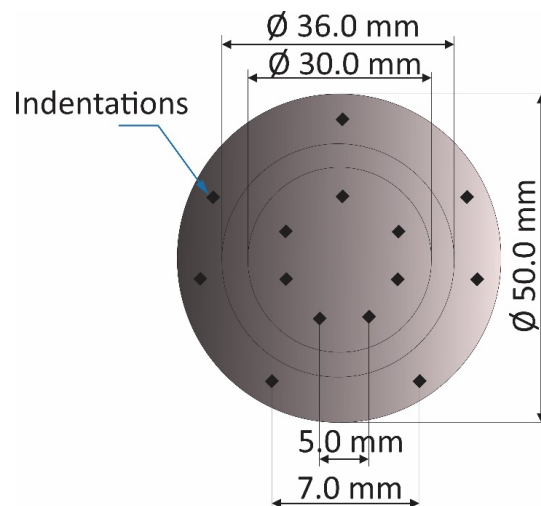
Figure 2. Sketch of performed Vickers microhardness indentations and worn tracks on the sample.

At this point, it is important to highlight that: there was a need to grind the samples surfaces after the deposition and also deposition followed by remelting process, to achieve the required surface roughness for the pin-on-disk tribological test (ASTM G99 - Ra: 0.8 µm). To ensure that the remelted layer was not removed, the following procedure was carried out. The parameter used in the coatings deposition (full description in topic 2.2.) resulted in layers with an average height of approximately 1.5 mm. Regarding the waviness (difference between peak and valley), the as-deposited condition showed

approximately 0.30 mm, while the remelted condition exhibited approximately 0.15 mm. It is important to highlight that both height and waviness values were measured approximately in the image J® software. The grinding process was employed to remove the waviness, so that, when the surface proved to be flat, the respective machining process was interrupted. Thus, the final average layer's height was around 1.2 mm (as-deposited) and 1.35 mm (remelted). As the remelting was applied immediately after deposition process conclusion (while the samples were still hot), with the same parameters (power and scanning speed), however, with powder feeder off, it is probably that laser beam has penetrated deeply into the layer, completely melting it. In this way, grinding process removed only a small remelted layer portion (that is, approximately 0.15 mm).

In previous works developed by the LMP-Laser group, consistent results are reported: Pôrto et al. (2019) performed a methodology for parameterizing the remelting process of single beads deposited via LMD and observed that throughout the evaluated parameter window, especially those deposited with higher energy, resulted in complete single bead remelting. Pereira et al. (2017), in the remelting evaluation applied in the misorietated volume reduction for turbine blades, they highlight similar behavior, as well as in the work, of similar objective, presented by Rottwinkel et al. (2017). Cao and Gu (2015), when evaluating density ratio, microstructures, and performance of TiC / Inconel 625 nanocomposites deposited via LMD, they observed that when increasing the energy, operating temperature is high enough to increase melt pool temperature and reduce the liquid viscosity, improving wettability. In this way, remelting process was able to encompass the layer's entire thickness. Besides that, the layer's waviness has been reduced considerably.

Another indicator in this regard concerns cooling cracks elimination in the remelted condition. Cracks of this nature were identified only in the as-deposited condition samples (this subject will be further discussed in topic 3). These cracks absence proves that the remelting treatment acted on the deposited layer entire thickness for two specific reasons: 1 - these cracks originate from the substrate, so if remelted condition did not present any cracks, it means that there was a sufficiently high melting to reach this region; 2 - even if cracks were only covered (due to the remelting transport effect, material reallocation), it is a sign that there was enough penetration in the other layers regions to generate this material displacement. Besides that, the fact that remelting posttreatment was applied immediately after the coatings deposition reduced the thermal gradient effect (tensile stresses resulting from the cooling process), contributing to this cracks elimination. In the results step (topic 3), authors will be indicated, such as Houdková et al. (2014) and Zhao et al. (2018), that report similar characteristics. Before and after tribological test, samples were cleaned in ethyl alcohol and dried.

With the tribometer calibrated, the pin-on-disk test in dry medium was carried out, aiming to reproduce actual two bodies wear. The Ni-Cr-B-Si coated discs were used as body and the aluminum oxide ball (Al_2O_3 - Ø 6 mm) as counter body. The data generated in the tests was acquired through LABVIEW® software. The following test parameters were used: normal load, 10 N; sliding speed, 0.5 m/s; as well as two sliding distance values: 1000 m and 1200 m. Relative humidity and ambient temperature were monitored during the tests. As well as the laser deposition parameters, the pin-on-disk tribological test parameters were defined based on preliminary tests and on literary research (see item 2.1., paragraph 2). The difference in the sliding test distance (1000 and 1200 m) is due to the different worn track diameters (Ø 30 mm and Ø 36 mm, respectively), to ensure that the cycle's number performed is similar.

From the experiments performed, the following results were measured or calculated: Khruschov (1957) H_a/H ratio; volumetric loss (via optical interferometry); k coefficient through the Equation 1 Archard (1953) model; friction coefficient (COF), measured by a load cell PW4MC3-30 N. The worn surfaces aspects and chemical composition, counter bodies and debris were analyzed via scanning electron microscope (SEM) and energy dispersive spectroscopy (EDS) in a HITACHI® TMC 3030, respectively.

$$k = \frac{Q}{(Ln*D)} \tag{1}$$

where: Q = volumetric loss (mm^3); k = Archard's wear coefficient [$mm^3/(Nm)$]; Ln = normal load (N) and D = sliding distance (m).

3. Results and Discussions

3.1. Surface aspects and coatings microhardness

The coatings showed good surface quality concerning the layer continuity and irregularities absence (such as waviness and depressions). The remelted surface aspect was even better compared to the as-deposited surface since the first did not exhibit unmelted powder particles and showed a lower waviness level (see topic 2.1., paragraph 2) compared to the latter (Rottwinkel et al., 2017; Pôrto et al., 2019). Besides that, none of the coating samples (both as-deposited and remelted) did not show material detachments during the tribological test performed (results of which will be presented and discussed in topics 3.2. and 3.3.). In as-deposited condition, some cracks were identified on the coating surface. The cracks arrangement in the direction perpendicular to the disk's diameter (which was also the same deposition direction used in this work, where the

samples were deposited in a circular strategy) indicates that these cracks may be resultant of the high tensile stresses resulting from the cooling process. The samples (disks) were deposited on a flat table (according to the Figure 1 illustrative scheme). During the cooling process, the samples first experience a compressive stress cycle, which tends to cause them to compress. Soon after, the samples begin to undergo tensile stresses, which cause them to expand. At this point, cooling cracks nucleation begins. This phenomenon is described by Kou (2003). This problem was not identified in the samples that were submitted to laser remelting posttreatment. Figure 3 presents a view of a sample surface in the conditions: a) as-deposited and b) remelted.
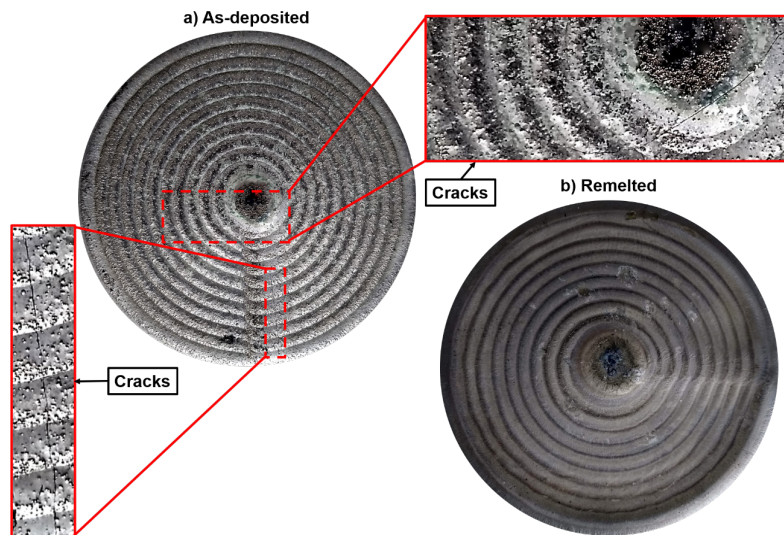
Figure 3. Sample surfaces characteristics: (a) as-deposited, highlighting the cooling cracks; and (b) remelted, where no cooling cracks were observed.

In the literature, Houdková et al. (2014) highlighted that during remelting process, a material portion is relocated by surface tension to the lower valleys concerning the plane. Zhao et al. (2018) indicate that this phenomenon can be easily understood when it is thought that the material of the roughness peaks is driven into the valleys, filling them, leaving a smooth and more leveled surface. In this research case, the cooling cracks resultant from the deposition process probably have been filled by this phenomenon. Moreover, it can be concluded that as the remelting was applied immediately after deposition conclusion, not enough time was allowed for significant temperature drop, thus such a high thermal gradient was not present, which is mainly responsible for cooling cracks nucleation and, therefore, no new cracks were nucleated.

Regarding microhardness values, the remelting treatment was also advantageous. Although the microhardness average (as-deposited - 582 HV_1 and remelted - 594 HV_1) difference between coatings conditions was small, punctual microhardness values along the total indentations set performed were more pronounced in remelted condition, confirming its best performance in this regard. The microhardness performance improvement is probably due to the internal void (like pores) reduction and to the increase in internal coating cohesion. Houdková et al. (2014) observed similar behavior in their research, attributing it to these same justifications. Besides that, in the present paper, this result may also be an indicator of the better reinforcement phases distribution (Cr carbides - CrC, identified via EDS) along the remelted coating surface (subject best discussed in topic 3.3). Figure 4 graph describes the microhardness behavior.
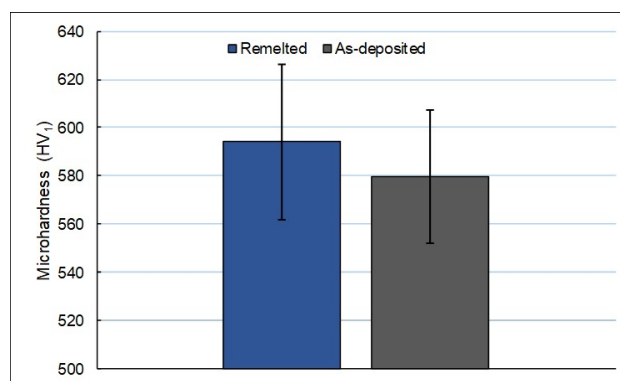
Figure 4. Coatings surface microhardness: as-deposited and remelted.

3.2. Friction coefficient, volumetric loss and *k* archard's coefficient

From the Khruschov (1957) relationship, both coating conditions underwent a severe wear regime (as-deposited - H_a/H: 3.5 and remelted - H_a/H: 3.4). It is important to note that this relation considered the average overall microhardness value of the coatings in their calculation. Thus, unlike the results obtained during the test (Figure 4), it is not possible to observe a significant difference. However, in real applications where a component is subjected to constant mechanical stresses, better uniformity of the mechanical properties distribution maybe even more important than the overall H_a/H value. The graph of Figure 4 showed that the remelted was more efficient in this regard.

The COF average over the test time for both conditions and sliding distances analyzed (1000 and 1200 m) was very similar (approximately 0.5, Figure 5). However, remelting treatment application showed a tendency of reduction in the oscillation of COF along with the test. Standard deviation analysis indicated, at both sliding distances evaluated, approximately 20% lower variation in the remelted to as-deposited condition. Similar results are reported by García et al. (2016) and Zhao et al. (2018).
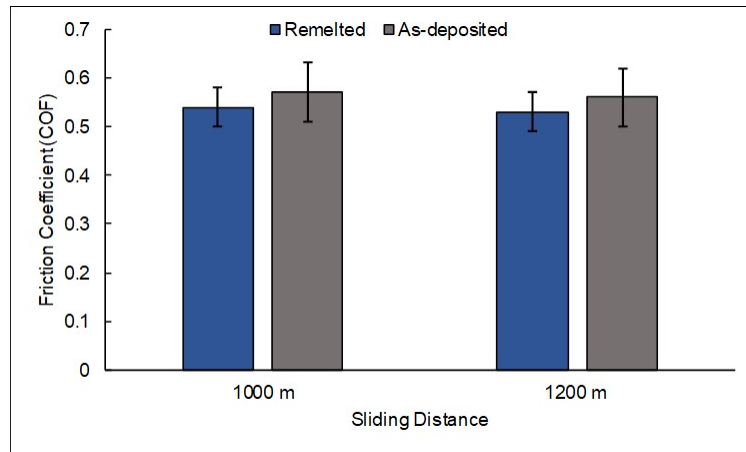
Figure 5. Coatings COF average: as-deposited and remelted.

Although as-deposited samples showed a tendency of inversely proportional relation between microhardness and wear rate, this behavior was more pronounced in the remelted coating. Thus, it is believed that the higher internal coating cohesion improved by laser remelting treatment also had a direct impact on this result. In the literature, Yin et al. (2011) and Zhao et al. (2018) report similar characteristics. Figure 6 shows the volumetric loss measured per section (five sections for each sample) for the different test sliding distances.
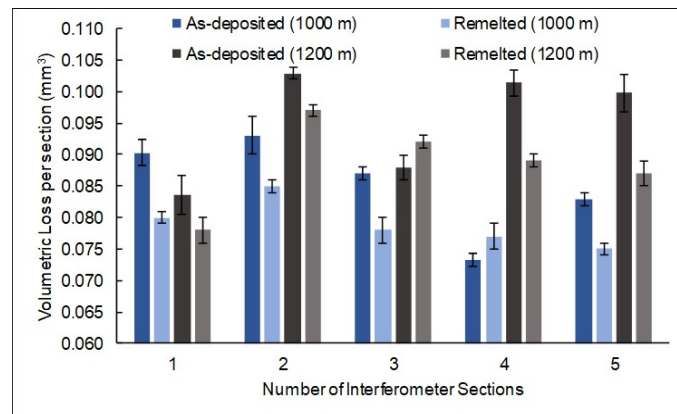
Figure 6. Volumetric loss per section × coating condition: as-deposited and remelted.

The graph of Figure 7 shows the cumulative average volumetric loss over the total test time, where it is possible to perceive the difference in a more quantitative way. In both sliding distances analyzed, especially for 1000 m, there is a tendency for the as-deposited condition to underperform the remelted condition. Probably, this behavior could intensify if the applied tribological testing conditions were even more severe. Besides that, remelted standard deviation was lower than that of as-deposited condition, which indicates its better uniformity of mechanical and tribological properties distribution along with the coating thickness, corroborating also it is lower volumetric loss evaluated punctually in the graph of Figure 6.
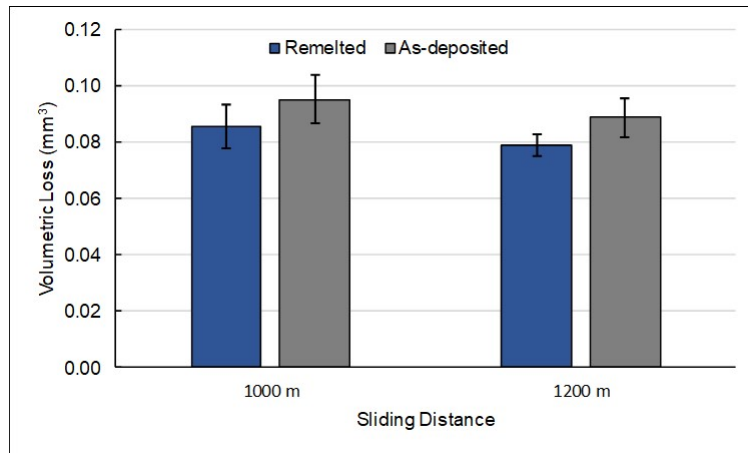
Figure 7. Accumulated volumetric loss over the total test time: as-deposited and remelted.

As the load and sliding distance was kept constant, the k Archard coefficient presented a correlation with the volumetric loss results (Figure 8). However, some particularities can be observed to the volumetric loss (Figure 6). First, remelted coating presented lower k values at most of the measurement points, whereas in Figure 6, this behavior was only identified for 1000 m sliding distance. Besides that, in Figure 6, volumetric loss was higher in the as-deposited condition at 1200 m sliding distance and lowest for the remelted at 1000 m sliding distance. In Figure 8 and Figure 9, on the other hand, the highest k coefficient was for as-deposited condition at 1200 m sliding distance and the lowest was for the remelted at 1200 sliding distance.
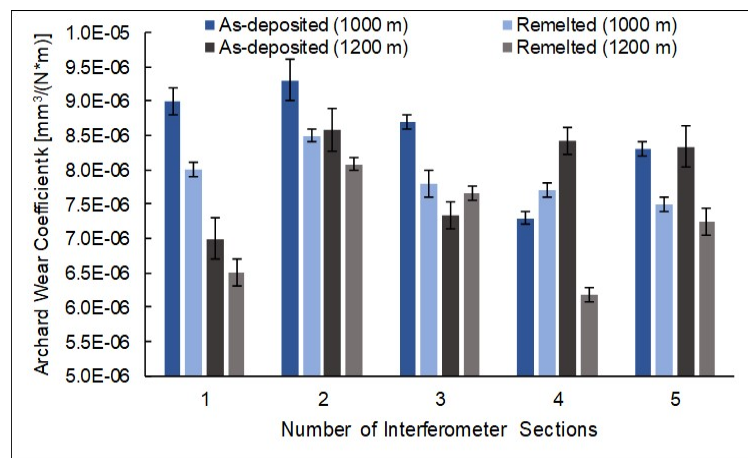
Figure 8. Archard wear coefficient per section × coating condition: as-deposited and remelted.
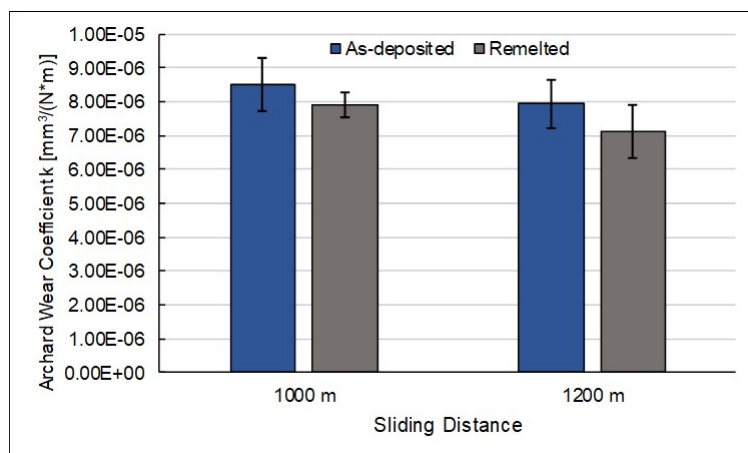
Figure 9. Accumulated Archard wear coefficient for both conditions and sliding distances: as-deposited and remelted.

In general, the remelting treatment application showed a positive contribution tendency in reducing the volumetric loss and k wear coefficient by approximately 12%. This result was observed at both sliding distances analyzed. This behavior proved to be compatible with surface characteristics, hardness, and defects absence. The punctual variations found, especially in the graph of Figure 8, are probably related to the wear micromechanisms behavior that acted on the tribological pair. This and the other interactions identified will be further discussed throughout topic 3.3.

3.3. Worn surfaces analysis

Figure 10 shows worn surfaces of the coatings with and without remelting treatment, highlighting the wear micromechanisms types identified: a) as-deposited coating worn surface shows adhesive wear, microploughings, chromium carbides (CrC), tribolayers and coating detachment; b) remelted coating worn surface, on the other hand, presents only CrC and a few adhesion and oxidation points.
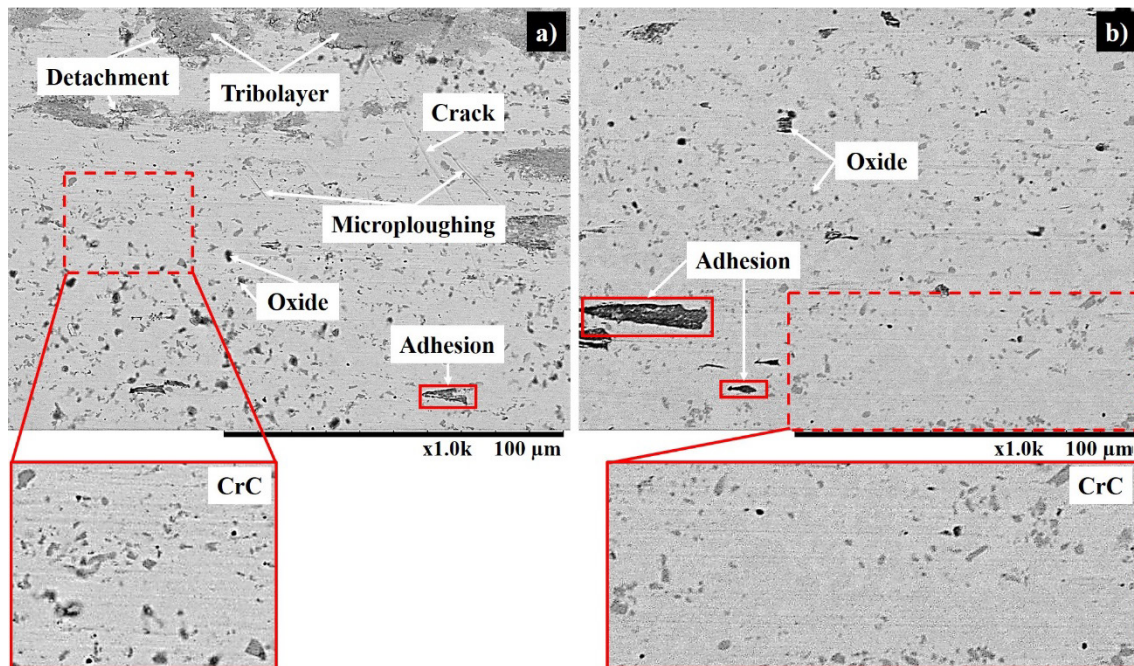
Figure 10. Worn surfaces images (1000 m sliding distance) obtained via MEV: (a) as-deposited; and (b) remelted.

Analyzing Figure 10, characteristic two bodies wear micromechanisms, adhesion and oxides are noticed in both the analyzed conditions. However, the action of these was more pronounced in as-deposited condition that, besides these, presented other mechanisms including characteristics of three bodies wear, like microploughing. In Figure 10a, although there are fractured CrC phases, there is no clear microcuttings evidence. As these phases have a much higher hardness than the matrix, loose particles acting as interfacial element could have increased the wear severity.

Besides to the less severe worn surface aspect, concerning CrC precipitates, in the remelted condition, CrC anchoring in the matrix was more efficient when compared to the as-deposited condition, avoiding phases detachments and increasing the restraint effect, which interrupts and/or hampers microploughings advancement; a phenomenon that goes back to Zum Gahr (1987) wear micromechanisms model. In the literature, similar results regarding the reinforcement phases behavior are indicated in several works (Colaço and Maranho, 2014; Houdková et al., 2014; Férnandez et al., 2015; García et al., 2016; Deschuyteneer et al., 2017; Sousa et al., 2020).

Figure 10 also made it clear that the active wear micromechanisms action was relatively contained from condition to the other. However, two factors identified only in as-deposited condition indicated the main causes of the higher wear rate presented then: tribolayers detachment and coating material detachment close to the cooling cracks.

In the literature, it is found that the tribolayers presence is advantageous due to its lubricating effect, where they act as an interfacial element, reducing the direct contact between body and counter body (Hutchings and Shipway, 2017). There are experimental studies that indicate the observation of this behavior (Silva and D'Oliveira, 2016). In this research, these elements presence, identified only in as-deposited coating for 1000 m sliding distance, contributed to the COF stabilization. However, tribolayers detachment was identified as a significant detrimental influence on their wear rate. Although no tribolayers was detected for 1200 m sliding distance, as the wear rate of both sliding distances was similar, it is believed that these tribolayers were removed along test time through the tribological pair interaction, and not by removal of more coating material. Figure 11a

shows an approximate image of condition 1's worn surface, where it is possible to perceive: 1 - tribolayer detachment, 2 - cooling cracks and 3 - coating material detachment close to the latter. Figure 11b shows an EDS spectrum, indicating the oxidation generated in this region.
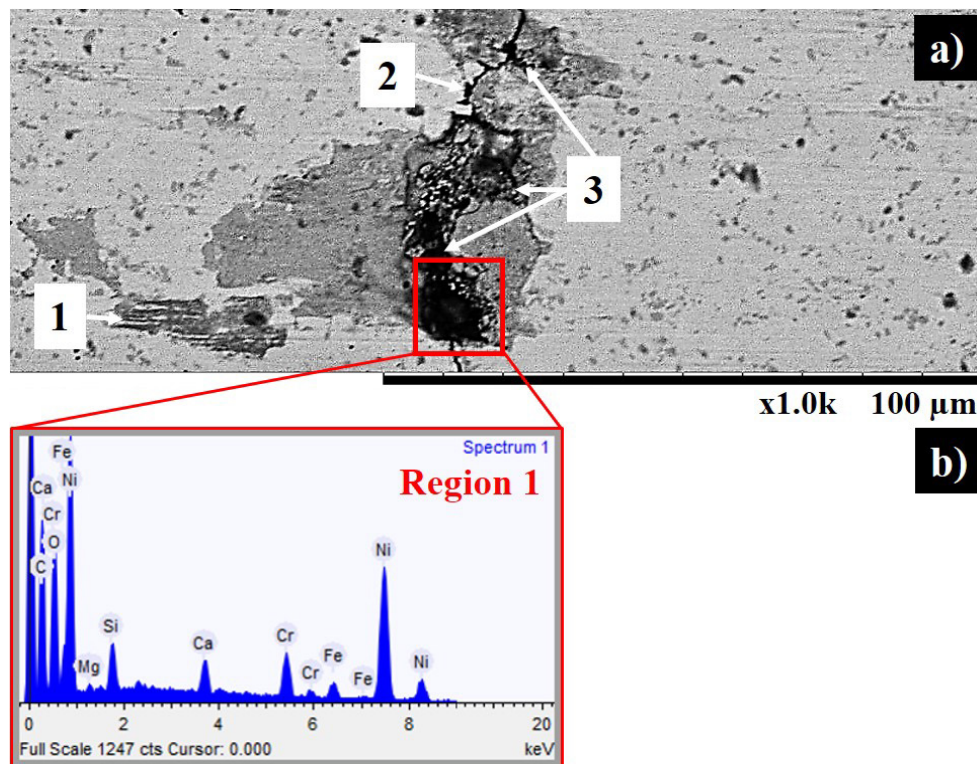
Figure 11. Worn surface: (a) 1 - tribolayer detachment, 2 - cooling cracks and 3 - coating material detachment close to the cooling cracks; (b) EDS spectrum.

Figure 11 made it clear that the cooling cracks impaired the as-deposited coating performance concerning remelted condition. The presence of this defect caused detachment of coating and counter body material through the collision between the tribological pair at the time the ball goes through a cracked region, generating vibration, which increased COF oscillation. As the test proceeds, debris accumulation within the cooling cracks has generated fatigue collapses at these interfaces, removing coating fragments. The deteriorated ball surface has worn out the coating surface more severely, increasing volumetric loss and k coefficient. Besides that, part of the generated debris ended up being loose between tribological pair, establishing a three bodies wear interface, that may have generated a considerable part of the microploughings observed in Figure 10a.

Cooling cracks absence in remelted coating is probably due to the lower thermal gradient provided by remelting, which reduced thermal stresses of the cooling process, which is the nucleation source of these cracks. In this way, remelting treatment eliminated all the damage defects originating from these cracks, the most severe of which is the material removal and coating embrittlement. In the literature, several researches report obtaining similar problems arising from the cooling cracks presence in the coatings of this alloy class. A technique widely used to avoid nucleation of these cracks is the application of substrate preheating at different temperatures (Houdková et al., 2014; Férnandez et al., 2015; García et al., 2016). Remelting application is also evaluated in this sense (Gusarov et al., 2011; Yin et al., 2011). Some studies analyze coatings without treatments, investigating the cooling crack's effects on tribological behavior in a more extensive way (Sousa et al., 2020).

Optical interferometry analysis, used in the worn tracks volume loss evaluation, shows that the worn track's characteristics corroborate the values of volumetric loss and k coefficient. The area removed from remelted coating was lower than as-deposited coating. Maximum average worn track depth of remelted (10 µm) was also lower than that of as-deposited (13 µm). Besides that, worn track irregularity of as-deposited coating was also higher than remelted coating, a result that may be related to the cooling cracks and the removal of some CrC phases present on its surface, which generated abrasion. This factor also reveals higher uniformity on the surface treated by remelting. Higher penetration depth and higher worn track irregularity of as-deposited coating corroborate the values of volumetric loss and k coefficient, presented previously in the graphs of Figure 7, Figure 8 and Figure 9, respectively. Figure 12 shows worn tracks characteristic sections, both for 1000 m sliding distance: a) as-deposited and b) remelted.
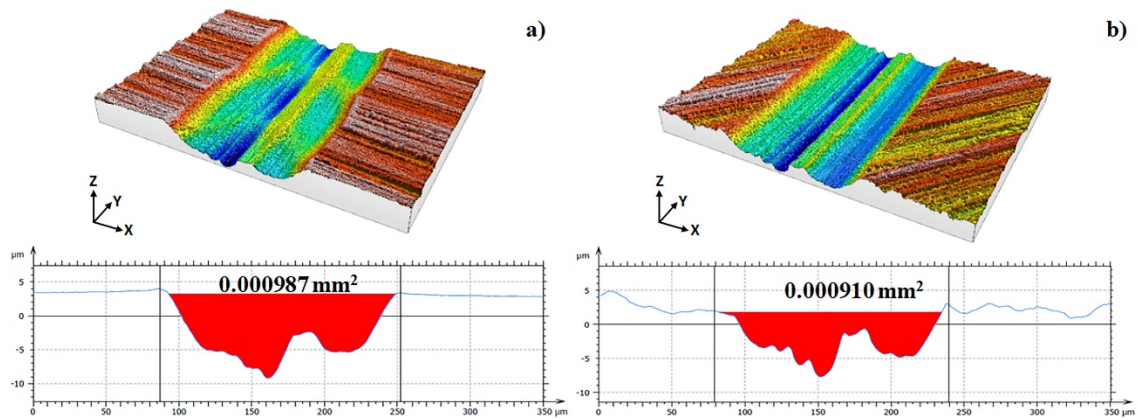
Figure 12. Track sections worn for 1000 m sliding distance: (a) as-deposited; and (b) remelted.

In both conditions of coating and sliding distances evaluated, there was no significant difference in wear of the balls used as counter body. Thus, it is possible to infer that only material removed from the coating contributed to the tribolayers formation, the effects of which were previously described. As shown in Figure 13, in the balls body, three phenomena were identified: coating adhesion (more and less severe); detachment and re-adhesion of the ball material itself (Al_2O_3); and less severe adhesion regions (Figure 13a), probably due to direct contact between CrC phases or cooling cracks during the test. In literature, Férnandez et al. (2015) highlight the achievement of similar results. Diameter of the worn shell was practically equal in both conditions evaluated.
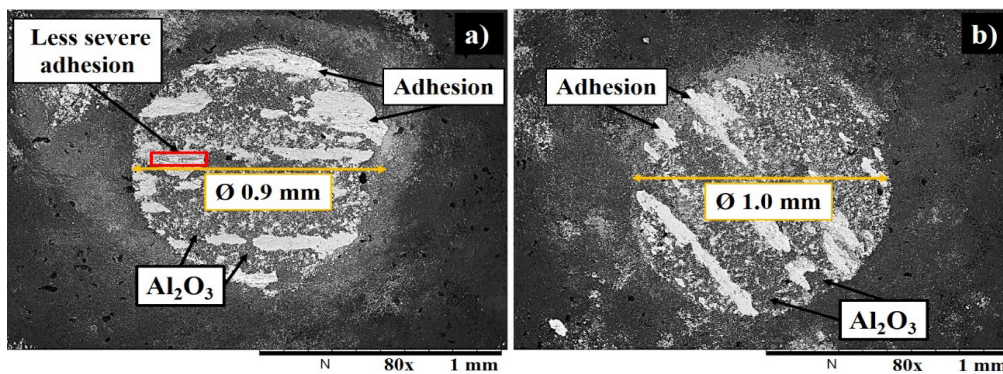
Figure 13. Worn surface of balls used as counter body: (a) as-deposited; and (b) remelted.

An evaluation of the debris generated along with the tribological tests (Figure 14a), a great dispersion of morphology and size was observed, where no characteristic patterns were identified. By the Khruschov (1957) ratio, both coatings conditions evaluated presented a severe wear regime, a factor that might have contributed to this result. EDS spectrum of these (Figure 14b) revealed metallic oxides aspects, category to which they are attributed in the literature (Silva and D'Oliveira, 2015, 2016).
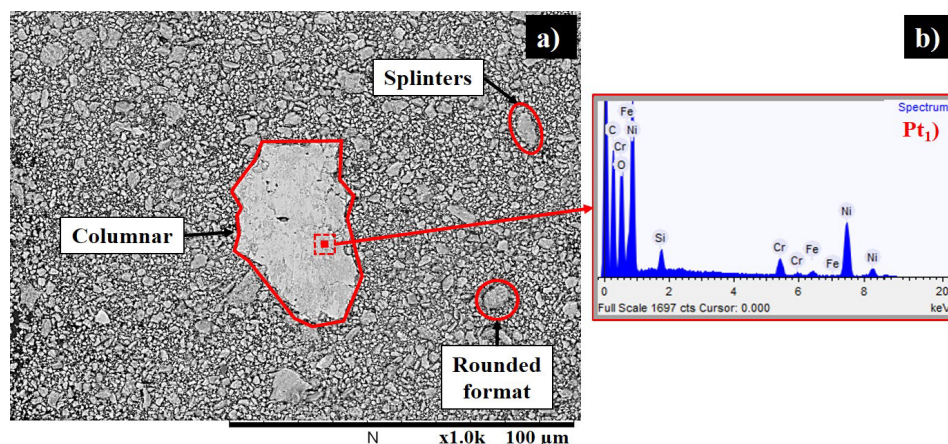
Figure 14. Debris generated during the tribological test: (a) general characteristics; and (b) EDS spectrum (Pt_1 - Point 1).

In general, the various aspects evaluated of worn surfaces are consistent with results of surface characteristics, hardness, and tribological behavior.

4. Conclusions

This paper evaluated the laser remelting posttreatment effects on tribological performance in the dry-sliding condition of a Ni-Cr-B-Si coating deposited via LMD. From the results obtained, it was possible to conclude that:

- The laser remelting posttreatment exerted a beneficial effect on the surface finish improvement, eliminating the unmelted powder particle's presence, reducing the waviness level and other characteristic defects, such as voids and depressions;

- Although the general COF average value did not change, the remelting showed a tendency to reduce its oscillation during the tribological test;

- The average values of volumetric loss and Archard wear coefficient showed a reduction tendency in the condition treated by laser remelting;

- In general, the worn surface's aspects were less severe in the laser remelted condition;

- Regardless of the coating condition evaluated, there was a tendency towards a reduction in the tribolayers presence with the sliding distance increase;

- Worn tracks dimensional characteristics observed through optical interferometry were compatible with the levels of volumetric loss and Archard wear coefficient;

- The wear of the balls used as counter body was similar in both evaluated coating conditions;

- Debris evaluation of both coating conditions did not show particular patterns of dimension, morphology or chemical composition;

- Coating material loss due to the tribolayers damage and the material detachment close to the cooling cracks were identified as the main negative influence causes on the tribological behavior;

- In general, the laser remelting posttreatment application on the Ni-Cr-B-Si coating deposited by LMD showed a tendency to improve its tribological behavior, mainly concerning worn surfaces aspects. Thus, it is possible to conclude that this treatment application tends to present even more pronounced advantages when this coating is subjected to more severe tribological testing conditions. In practice, this improvement may mean an increase in the lifespan and/or components performance.

Acknowledgements

References

American Society for Testing and Materials. ASTM-E92: standard test methods for vickers hardness and Knoop hardness of metallic materials. Pensilvânia: ASTM; 2017a. 27 p.

American Society for Testing and Materials. ASTM-G99: standard test method for wear testing with a pin-on-disk apparatus. Pensilvânia: ASTM; 2017b.

Archard J. Contact and rubbing of flat surfaces. Journal of Applied Physics. 1953;24(8):981-988. http://dx.doi.org/10.1063/1.1721448.

Borges B, Quintino L, Miranda RM, Carr P. Imperfections in laser clading with powder and wire fillers. International Journal of Advanced Manufacturing Technology. 2010;50(1-4):175-183. http://dx.doi.org/10.1007/s00170-009-2480-2.

Cao S, Gu D. Laser metal deposition additive manufacturing of TiC/Inconel 625 nanocomposites: relation of densification, microstructures and performance. Materials Research. 2015;30(23):3616-3628. http://dx.doi.org/10.1557/jmr.2015.358.

Chen J, Li J, Song R, Bai LL, Shao JZ, Qu CC. Effect of the scanning speed on microstructural evolution and wear behaviors of laser cladding NiCrBSi composite coatings. Optics & Laser Technology. 2015;72:86-99. http://dx.doi.org/10.1016/j.optlastec.2015.03.015.

Colaço FHG, Maranho O. Avaliação da perda de massa de revestimento duro depositado por soldagem com arame tubular de liga FeCrC-Ti. Soldagem e Inspeção. 2014;19(1):58-68. http://dx.doi.org/10.1590/S0104-92242014000100008.

Davim JP. Laser in manufacturing. 1st ed. New Jersey: John Wiley & Sons; 2013. http://dx.doi.org/10.1002/9781118562857.

Deschuyteneer D, Petit D, Gonon M, Cambier F. Influence of large particle size – up to 1.2mm – and morphology on wear resistance in NiCrBSi/WC laser cladded composite coatings. Surface and Coatings Technology. 2017;311:365-373. http://dx.doi.org/10.1016/j.surfcoat.2016.12.110.

Férnandez MR, García A, Cuetos JM, González R, Noriega A, Cadenas M. Effect of actual WC content on the reciprocating wear of a laser cladding NiCrBSi alloy reinforced with WC. Wear. 2015;324-325:80-89. http://dx.doi.org/10.1016/j.wear.2014.12.021.

García A, Férnandez MR, Cuetos JM, González R, Ortiz A, Cadenas M. Study of the sliding wear and friction behavior of WC + NiCrBSi laser cladding coatings as a function of actual concentration of WC reinforcement particles in ball-on-disk test. Tribology Letters. 2016;41(3):41. http://dx.doi.org/10.1007/s11249-016-0734-3.

Ghabchi A, Rombouts M, Holmberg K, Persoons R. "Microstructure and failure modes during scratch testing of laser cladded WC-NiCrBSi coatings with spherical and angular carbides". Tribology: Materials, Surfaces and Interfaces. 2013;7(1):13-20. http://dx.doi.org/10.1179/1751584X13Y.0000000023.

Gusarov AV, Pavlov M, Smurov I. Residual stresses at laser surface remelting and additive manufacturing. physics procedia. 2011;12:248-254. http://dx.doi.org/10.1016/j.phpro.2011.03.032.

Hemmati I, Ocelík V, Csach K, De Hosson JTM. Microstructure and phase formation in a rapidly solidified laser-deposited Ni-Cr-B-Si-C hardfacing alloy. Metallurgical and Materials Transactions A: Physical Metallurgy and Materials Science. 2014;45(2):878-892. http://dx.doi.org/10.1007/s11661-013-2004-4.

Hemmati I, Ocelík V, De Hosson JTM. Dilution effects in laser cladding of Ni–Cr–B–Si–C hardfacing alloys. Materials Letters. 2012;84:69-72. http://dx.doi.org/10.1016/j.matlet.2012.06.054.

Hemmati I, Ocelík V, De Hosson JTM. Effects of the alloy composition on phase constitution and properties of laser deposited Ni-Cr-B-Si coatings. Physics Procedia. 2013;41:302-311. http://dx.doi.org/10.1016/j.phpro.2013.03.082.

Hemmati I, Ocelík V, De Hosson JTM. Evolution of microstructure and properties in laser cladding of a Ni-Cr-B-Si hardfacing alloy. Contact Mechanics and Surface Treatments X. 2011;71:287-296. http://dx.doi.org/10.2495/SECM110251.

Holmberg K, Andersson P, Erdemir A. Global energy consumption due to friction in passenger cars. Tribology International. 2012;47:221-234. http://dx.doi.org/10.1016/j.triboint.2011.11.022.

Holmberg K, Andersson P, Nylund N-O, Mäkelä K, Erdemir A. Global energy consumption due to friction in trucks and buses. Tribology International. 2014;78:94-114. http://dx.doi.org/10.1016/j.triboint.2014.05.004.

Holmberg K, Erdemir A. Influence of tribology on global energy consumption, costs and emissions. Friction. 2017;5(3):263-284. http://dx.doi.org/10.1007/s40544-017-0183-5.

Holmberg K, Kivikytö-Reponen P, Härkisaari P, Valtonen K, Erdemir A. Global energy consumption due to friction and wear in the mining industry. Tribology International. 2017;115:116-139. http://dx.doi.org/10.1016/j.triboint.2017.05.010.

Houdková Š, Smazalová E, Vostřák M, Schubert J. Properties of NiCrBSi coating, as sprayed and remelted by different technologies. Surface and Coatings Technology. 2014;253:14-26. http://dx.doi.org/10.1016/j.surfcoat.2014.05.009.

Hutchings I, Shipway P. Tribology: friction and wear of engineering materials. 1st ed. Cambridge: Butterworth-Heinemann; 2017.

Kaiming W, Yulong L, Hanguang F, Yongping L, Zhenqing S, Pengfei M. A study of laser cladding NiCrBSi/Mo composite coatings. Surface Engineering. 2016;34(4):267-275. http://dx.doi.org/10.1080/02670844.2016.1259096.

Khruschov MM. Resistance of metals to wear by abrasion, as related to hardness. In: Proceedings of the Conference on Lubrication and Wear; 1957; London. London: American Society of Mechanical Engineers; 1957.

Kou S. Welding metallurgy. 2nd ed. New Jersey: John Wiley & Sons; 2003.

Marimuthu S, Triantaphyllou A, Antar M, Wimpenny D, Morton H, Beard M. Laser polishing of selective laser melted components. International Journal of Machine Tools & Manufacture. 2015;95:97-104. http://dx.doi.org/10.1016/j.ijmachtools.2015.05.002.

Ocelík V, Nenadl O, Palavra A, De Hosson JTM. On the Geometry of coatings layers formed by overlap. Surface and Coatings Technology. 2014;242:54-61. http://dx.doi.org/10.1016/j.surfcoat.2014.01.018.

Pereira ASP, Rottwinkel B, Kaierle S, Weingaertner WL, Wesling V. Laser remelting as mean to reduce clad misorietated volume deposited throught laser cladding when applied to single cristaline turbine blades. In: Anais do IX Congresso Brasileiro de Engenharia de Fabricação; 2017; Joinville. Rio de Janeiro: Associação Brasileira de Ciências Mecânicas; 2017.

Pôrto RM, Pereira ASP, Pereira M. Parametrization methodology for laser remelting applied over laser metal deposition single tracks. In: Proceedings of the 38nd International Congress on Applications of Lasers & Electro-Optics (ICALEO 2019); 2019; Orlando, United States of America. Orlando: Laser Institute of America; 2019.

Rottwinkel B, Pereira ASP, Alfred I, Noelke C, Wesling V, Kaierle S. Turbine blade tip single crystalline clad deposition with applied remelting passes for well oriented volume expansion. Journal of Laser Applications. 2017;29(2):022310. http://dx.doi.org/10.2351/1.4983667.

Silva LJ, D'Oliveira ASCM. Liga NiCrBSiC: microestrutura e dureza de revestimentos processados a arco e a laser. Soldagem e Inspeção. 2015;20(1):39-47. http://dx.doi.org/10.1590/0104-9224/SI2001.05.

Silva LJ, D'Oliveira ASCM. NiCrSiBC coatings: effect of dilution on microstructure and high temperature tribological behavior. Wear. 2016;350-351:130-140. http://dx.doi.org/10.1016/j.wear.2016.01.015.

Sousa JMS, Ratusznei F, Pereira M, Castro RM, Curi EIM. Abrasion resistance of Ni-Cr-B-Si deposited by laser cladding process. Tribology International. 2020;143:106002. http://dx.doi.org/10.1016/j.triboint.2019.106002.

Sousa JMS. Análise das propriedades tribológicas de revestimentos de de Ni-Cr-B-Si depositados via laser cladding a pó [dissertação]. Faculdade de Engenharia Mecânica, Universidade Federal de Santa Catarina, Florianópolis; 2019.

Stanciu EM, Pascu A, Tierean MH, Voiculescu I, Roatã IC, Croitoru C, et al. Dual coating laser cladding of NiCrBSi and inconel 718. Materials and Manufacturing Processes. 2016;31(12):1556-1564. http://dx.doi.org/10.1080/10426914.2015.1103866.

Temmler A, Willenborg E, Wissenbach K. Design surfaces by laser remelting. Materialwissenschaft und Werkstofftechnik. 2015;46(7):692-703. http://dx.doi.org/10.1002/mawe.201500345.

Toyserkani E, Corbin S, Khajepour A. Laser cladding. 1st ed. Florida: CRC Press LLC; 2005.

Weng Z, Wang A, Wu X, Wang Y, Yang Z. Wear resistance of diode laser-clad Ni/WC composite coatings at different temperatures. Surface and Coatings Technology. 2016;304:283-292. http://dx.doi.org/10.1016/j.surfcoat.2016.06.081.

Yin B, Zhou HD, Chen JM, Yan FY. Microstructure and high temperature sliding wear behaviour of laser remelted NiCrBSi/35(WC-12Ni) composite coating. Surface Engineering. 2011;27(6):458-463. http://dx.doi.org/10.1179/026708410X12687356948517.

Zhao Y, Sun J, Guo K, Li J. Investigation on the effect of laser remelting for laser cladding nickel based alloy. In: Proceedings of the 37nd International Congress on Applications of Lasers & Electro-Optics (ICALEO 2018); 2018; Orlando, United States of America. Orlando: Laser Institute of America; 2018. http://dx.doi.org/10.2351/1.5096126.

Zhong M, Liu W. Laser surface cladding: the state of the art and challenges. Journal of Mechanical Engineering Science. 2010;224(5):1041-1060. http://dx.doi.org/10.1243/09544062JMES1782.

Zum Gahr, K.-H. Microstructure and ear of materials. 1st ed. New York: Elsevier Science; 1987.